Tailoring Complex Weld Geometry through Reliable Heat-Transfer and Fluid-Flow Calculations and a Genetic Algorithm

A. KUMAR and T. DEBROY

Systematic tailoring of weld attributes based on scientific principles is an important goal in fabricating reliable welds. What is needed, and is not currently available, is the ability to systematically determine multiple welding-variable sets to achieve a target weld feature such as geometry. Here, we show how the transport phenomena–based models can be completely restructured to achieve this goal. First, the reliability of the heat-transfer and fluid-flow model predictions is increased by optimizing the values of uncertain input variables such as the arc efficiency from a limited volume of experimental data. Next, after the model predictions are made reliable, the numerical heat-transfer and fluid-flow model is coupled with a genetic algorithm (GA) to achieve bidirectionality of the model and to determine multiple pathways to achieve a specified weld attribute such as the weld geometry. The proposed approach is demonstrated in complex gas metal-arc (GMA) fillet welding of low-alloy steel, for which various sets of welding variables are computed to achieve a specified weld geometry. The model predictions are compared with appropriate independent experimental results. The modeling results, apart from providing definitive insight regarding the complex physics of welding, also provide hope that weld attributes can be tailored reliably through multiple routes based on heat-transfer and fluid-flow calculations and evolutionary algorithms.

I. INTRODUCTION

IN recent years, complex numerical models of heat transfer and fluid flow for various fusion-welding processes such as the gas tungsten-arc welding,[1,2,3] gas metal-arc (GMA) welding,[4–7] and laser welding[8,9,10] have been developed to better understand the physical processes in welding and the nature of the welded materials. These models have enabled accurate quantitative calculations of thermal cycles and fusion-zone geometry that have been used to quantitatively understand various attributes of the welded joints like weld metal-phase composition,[11,12] grain structure,[13,14] and inclusion structure.[15] Although these models have provided significant insight about the welding processes and welded materials, their applications have been limited due to several factors.

First, although these heat-transfer and fluid-flow models use time-tested equations of conservation of mass, momentum, and energy, their predictions of temperature fields and thermal cycles do not always agree with experimental results because the models require many input variables, all of which cannot be prescribed with certainty. For example, the reported values of arc efficiency vary significantly for apparently similar welding conditions, reflecting the complexity of the GMA welding process.[7,16–20] Values of arc efficiency significantly affect the results of numerical heat-transfer and fluid-flow calculations. Therefore, reliable predictions of temperature and velocity fields cannot be obtained without ascertaining accurate values of this and other uncertain parameters.[18,20–22] Second, the models are designed to calculate the temperature and velocity fields for a given set of welding variables. However, very often what is needed is to determine the welding variables required to achieve a given weld attribute such as the weld geometry. The current generation of unidirectional heat-transfer and fluid-flow models are designed to calculate temperature and velocity fields from welding conditions and are incapable of determining welding conditions. Finally, the GMA welding system is highly complex and involves nonlinear interaction of several welding variables. As a result, a particular weld attribute such as the geometry can be obtained *via* multiple paths, *i.e.*, through the use of various sets of welding variables. The current generation of numerical heat-transfer and fluid-flow models cannot determine alternative pathways to achieve a target weld attribute.

Here, we show that by combining numerical heat-transfer and fluid-flow models with a suitable optimization algorithm, the reliability of the model predictions can be significantly enhanced. Furthermore, the combined models now have new capabilities for bidirectional simulation, where either the traditional input or output variables can be specified. The new formulation also allows determination of multiple solutions to attain a specified weld attribute. First, the reliability of heat-transfer and fluid-flow models is increased by calculating the uncertain input parameters such as the arc efficiency, effective thermal conductivity, and effective viscosity. The values of these three unknown variables are calculated by coupling a conjugate-gradient optimization method[20] with three-dimensional heat-transfer and fluid-flow calculations and using a limited volume of experimental data. Here, the conjugate-gradient method is selected to improve the reliability of the heat-transfer and fluid-flow model because of the general lack of local minima in the objective function and rapid convergence.[7,20] The calculated weld geometry obtained by using the optimized values of the uncertain input parameters in the heat-transfer and fluid-flow model were compared with the corresponding

A. KUMAR, Graduate Student, and T. DEBROY, Professor, are with the Department of Materials Science and Engineering, The Pennsylvania State University, University Park, PA 16802. Contact e-mail: debroy@psu.edu

Manuscript submitted February 14, 2005.

experimental geometry to check the reliability of these calculations. Finally, the bidirectional capability of the heat-transfer and fluid-flow models is attained by coupling the heat-transfer and fluid-flow calculations with a genetic algorithm (GA).[23–27] The GA can systematically search for multiple combinations of welding-variable sets that comply with the phenomenological laws of welding physics and obtain a population of solutions following certain rules of evolution.[23–27] Furthermore, the capability to determine alternate paths to achieve a target weld geometry is demonstrated by estimating various sets of welding variables, *i.e.*, arc current (I), arc voltage (V), welding speed (U), and wire feed rate (w_f) that can all produce a target weld geometry.

The enhanced reliability of the calculation of heat transfer and fluid flow allows improved understanding of the physical processes of welding. In particular, the role of various driving forces for fluid flow on the weld geometry in the complex GMA welding is examined. The deformation of the free surface for various welding conditions is examined. The turbulent heat transfer and fluid flow in the weld pool is simulated by a vorticity-based one-equation turbulence model.[20,28,29] This turbulence model uses a variable mixing length to adequately consider an irregular and complex weld-pool geometry characterized by finger penetration and severe deformation of the weld pool under the arc.[20] The predictions of the vorticity-based model are compared with the zero-equation effective viscosity and effective-thermal-conductivity model. Good agreement was obtained between the values of these parameters calculated by the two models, indicating the effectiveness of the optimization scheme to determine the values of the effective thermal conductivity and viscosity. In short, this article shows that the proposed heat-transfer and fluid-flow model of GMA welding provides enhanced reliability of the computed results, providing improved insight into the complex physics of the GMA process, and shows that weld attributes can be tailored through multiple pathways based on scientific principles.

II. THE MATHEMATICAL MODEL

A. *Modeling of Heat Transfer and Fluid Flow during GMA Fillet Welding*

The main computational engine used here is a well-tested heat-transfer and fluid-flow model[5,6,20] that solves the equations of conservation of mass, momentum, and energy in three dimensions. This forward model takes into account the complex fillet joint shape, the deformation of the weld-pool top surface, heat transfer by the hot metal droplets, and the addition of the filler metal from the consumable electrode. Because of the complexity of the GMA fillet welding, the following simplifying assumptions[5,20] are made to make the computational work tractable.

(1) The liquid metal flow is assumed to be incompressible and Newtonian. The effect of turbulent flow in the weld pool is taken into account through the use of the enhanced thermal conductivity and viscosity of the liquid metal.[5,17,20] In some calculations, a vorticity-based one-equation turbulent model is used.
(2) The heat transported from the filler-metal droplets is taken into account using a time-averaged volumetric heat source.[4,5,7,30]
(3) Both the heat and current flux from the arc are assumed to have a Gaussian distribution at the weld-top surface. The distribution is unaffected by the deformation of the weld-pool top surface.[4,5,7]

More details of the numerical model of heat transfer and fluid flow of GMA fillet welding are available in the literature[5,20] and are not repeated here. Only the salient features specific to the current problem are outlined in brief.

The convection in the weld pool is driven mainly by the spatial gradient of interfacial tension and the electromagnetic force field and, to a much lesser extent, by the buoyancy force. By using a coordinate system attached to the heat source, the welding problem is assumed to be at steady state.[4,5] Therefore, the heat transfer and fluid flow during welding can be calculated by solving the following governing equations:[4,5]

$$\frac{\partial u_i}{\partial x_i} = 0 \qquad [1]$$

$$\rho \frac{\partial (u_i u_j)}{\partial x_i} = \frac{\partial}{\partial x_i}\left(\mu \frac{\partial u_j}{\partial x_i}\right) + S_j \qquad [2]$$

$$\rho \frac{\partial (u_i h)}{\partial x_i} = \frac{\partial}{\partial x_i}\left(\alpha \frac{\partial h}{\partial x_i}\right) - \rho L \frac{\partial (u_i f_l)}{\partial x_i} - \rho U_w \frac{\partial h}{\partial x_1} - \rho U_w L \frac{\partial f_l}{\partial x_1} + S_v \qquad [3]$$

Equations [1] through [3] are the continuity, momentum-conservation, and energy-conservation equations, respectively. In these equations, the subscripts i and j indicate the coordinate direction ($i, j = 1, 2$, and 3), x is the distance, u is the melt velocity, ρ is the density, μ is the viscosity, S_j is the source term for jth momentum equation, h is the sensible heat, α is the thermal-diffusion coefficient (defined as $\alpha = k/C_p$, where k is the thermal conductivity and C_p is the specific heat), U_w is the material moving speed (parallel to the positive x direction, *i.e.*, $i = 1$ direction), L is the latent heat of fusion, and S_v is a source term accounting for the additional heat from metal droplets. In Eq. [2], the source term S_j is given as

$$S_j = -\frac{\partial p}{\partial x_j} - \rho U_w \frac{\partial u_j}{\partial x_1} - C\left(\frac{(1-f_l)^2}{f_l^3 + B}\right) u_j + F_j^e + F_j^b \qquad [4]$$

where p represents the pressure, f_l is the liquid-metal fraction, and F_j^e and F_j^b correspond to the electromagnetic and buoyancy forces in the jth direction, respectively. Details about the calculation of the electromagnetic and buoyancy source terms are available in the literature.[4,5,7] In Eq. [4], the third term represents the frictional dissipation in the mushy zone according to the Carman–Kozeny approximation,[31] where B and C are two constants. The liquid-metal fraction is assumed to vary linearly with temperature:

$$f_l = \begin{cases} 1 & T \geq T_l \\ \dfrac{T - T_s}{T_l - T_s} & T_s < T < T_l \\ 0 & T \leq T_s \end{cases} \qquad [5]$$

where T_l and T_s are the liquidus and solidus temperature of the material, respectively. The complex joint shape and the severely deformed weld-pool surface in fillet welding require

the use of a deformable, curvilinear grid system for accurate calculation of heat transfer and fluid flow. Therefore, the governing equations are transformed from the Cartesian to curvilinear coordinate system.[4,5] The transformed governing equations are discretized using the control-volume method.[31] The discretized equations for enthalpy, three components of velocity, and pressure are formulated by integrating the corresponding governing equation over all the interior control volumes in the computational domain. These discretized governing equations are solved to obtain the temperature and velocity fields and the free-surface profile. First, the modified SIMPLE algorithm[32] is used to calculate the temperature and velocity fields. Then, the free-surface profile is calculated based on the temperature field obtained in the previous step. After the solution of the free-surface profile, the z locations of grids are adjusted to fit the surface profile, and the temperature and velocity fields are then recalculated in the fitted grid system. The calculation procedure is repeated until the converged temperature and velocity fields and free-surface profile are obtained.

A $72 \times 66 \times 47$ grid system was used, and the corresponding solution domain had dimensions of 450 mm in length, 108 mm in width, and 18 mm in depth. Spatially nonuniform grids with finer grids near the heat source were used for maximum resolution of variables. The calculations normally converged within 5000 iterations, which took about 30 minutes in a personal computer with a 3.06 GHz INTEL* P4 central processing unit and a 512 Mb PC2700 double data rate synchronous dynamic random access memory (DDR-SDRAM) memory.

*INTEL is a trademark of the Intel Corporation, Santa Clara, CA.

The three-dimensional temperature field in the GMA weld computed from the model is used to calculate the weld dimensions, *i.e.*, penetration, throat, and leg-length. An effective search for multiple welding-variable sets to attain a given geometry requires many runs of the heat-transfer and fluid-flow model. Only because of the recent advances in computational hardware and software can such a computationally intensive task for tailoring weld attributes be undertaken. The output from the model includes temperature and velocity fields, thermal cycles, fusion-zone geometry, and the solidified geometry of the weld reinforcement.

B. *GA as an Optimization Model*

The GA-based search for multiple sets of welding variables to achieve a target weld geometry starts with many initial sets of randomly chosen values for the four most important welding variables, *i.e.*, current, voltage, welding speed, and the wire feed rate. A systematic global search is next undertaken to find multiple sets of values for these four welding variables that lead to the least error between the calculated and the target weld dimensions, *i.e.*, penetration, throat, and the leg length. The heat-transfer and fluid-flow model calculates the values of these weld dimensions for each set of input welding variables. The chosen values of welding variables do not always produce the desired weld dimensions, and the resulting mismatch between the computed and the desired weld dimensions is expressed by the following objective function ($O(f)$):

$$O(f) = \left(\frac{p^c}{p^t} - 1\right)^2 + \left(\frac{t^c}{t^t} - 1\right)^2 + \left(\frac{l^c}{l^t} - 1\right)^2 \qquad [6]$$

where p^c, t^c, and l^c are the computed penetration, throat, and the leg length of the weld bead, respectively, and p^t, t^t, and l^t are the corresponding target or desired values of these three parameters. The objective function depends on four main welding variables: current, voltage, welding speed, and the wire feed rate.

$$O(f) = O(f_1, f_2, f_3, f_4) = O\left(\frac{I}{I_r}, \frac{V}{V_r}, \frac{U}{U_r}, \frac{w_f}{(w_f)_r}\right) \qquad [7]$$

In Eq. [7], the reference values I_r, V_r, U_r, and $(w_f)_r$ represent the order of magnitude of the welding variables. Note that Eq. [7] is made nondimensional to preserve the importance of all four welding variables by making their nondimensional values comparable in magnitude. The GA produces new individuals, or sets of welding conditions, with iterations based on the evolutionary principles.[23–27,32] The GA used in the present study is a parent-centric recombination (PCX) operator–based generalized generation gap (G3) model.[25,26,27] The generic PCX operator is a steady-state, elite-preserving, scalable, and computationally fast population-alteration model. This model was chosen because it has been shown to have a faster convergence rate on standard test functions as compared to other evolutionary algorithms and classical optimization algorithms, including other real-parameter GAs with the unimodal normal distribution crossover and the simplex crossover operators, the correlated self-adaptive evolution strategy, the covariance-matrix adaptation evolution strategy, the differential evolution technique, and the quasi-Newton method.[26] A detailed description of this model is available in the literature[24–27] and is not included here. The multiple deme (or island)–based parallelized GA model[24,33] used in the present study helps in faster exploration of the window of welding parameters by dividing the search space and migrating the best solutions to all the other processors. Selection of the emigrants and replacements based on their fitness enhances the selection process, which increases the speed of convergence. If the selection is too weak, the population may drift aimlessly for a long time, and the quality of the solutions may not be good.[33] Therefore, the selection intensity is chosen high in this algorithm by migrating the best individuals from one processor and replacing the worst individuals on the neighboring processors. The population converges to a set of optimal solutions through an iterative scheme involving a PCX operator–based recombination scheme. The specific application of this model for the GMA welding process is described in Appendix A. The ability of the GA to find multiple optimal solutions independent of the initial guessed values[24–27] makes it unique for estimating the window of welding parameters.

III. RESULTS AND DISCUSSION

A. *Effect of the Various Driving Forces on the Weld-Pool Geometry*

During GMA welding, several driving forces act on the liquid metal in the weld pool.[1,2,5] In the heat-transfer and fluid-flow model, the electromagnetic, Marangoni, and buoyancy forces were considered in the calculations.[1,2] The calculated temperature and velocity fields, when all three driving forces are considered, are shown in Figure 1. The material

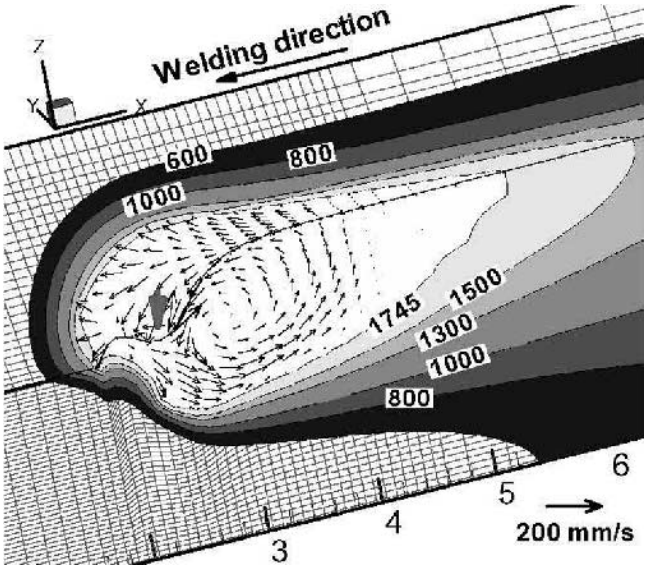

Fig. 1—Calculated temperature and velocity fields in GMA fillet weld for an arc current of 362.0 A, arc voltage of 33 V, welding speed of 4.2 mm/s, and wire feed rate of 211.7 mm/s. All the temperatures are given in Kelvin. The vertical arrow in the middle of the weld pool indicates the location of the heat source. The weld-pool boundary is represented by the 1745 K isothermal line.

Table I. Physical Properties of the A-36 Steel and the Other Data Used in the Calculation

Name	Value
Liquidus temperature, T_l (K)	1785.0
Solidus temperature, T_s (K)	1745.0
Density of metal, ρ (kg m^{-3})	7800
Thermal conductivity of solid, k_s (J m^{-1}·s^{-1}·K^{-1})	21.0
Enhanced thermal conductivity of liquid, k_l (J m^{-1}·s^{-1}·K^{-1})	88.2
Enhanced viscosity of liquid metal, μ (kg m^{-1} s^{-1})	3×10^{-2}
Specific heat of solid, C_{ps} (J kg^{-1}·K^{-1})	703.4
Specific heat of liquid, C_{pl} (J kg^{-1}·K^{-1})	808.1
Surface tension of liquid metal, γ (N m^{-1})	1.2
Temperature coefficient of surface tension, $d\gamma/dT$ (N m^{-1}·K^{-1})	-0.35×10^{-3}
Magnetic permeability, μ_m (N A^{-2})	1.26×10^{-6}
Ambient temperature, T_a (K)	298 K

properties used in the calculation are listed in Table I. For clarity, only half of the workpiece is shown, since the weld is symmetric about the central longitudinal plane containing the welding direction. As shown in this figure, the liquid-metal motion is quite complicated due to the combined effect of the driving forces. The electromagnetic force plays a dominant role in driving the liquid-metal flow in the weld pool.[5] In the middle of the weld pool, the liquid metal is driven downward by the electromagnetic force, and a major counterclockwise circulation loop is formed along the central longitudinal plane. On the other hand, at the top surface of the weld pool, the Marangoni shear stress drives the melt

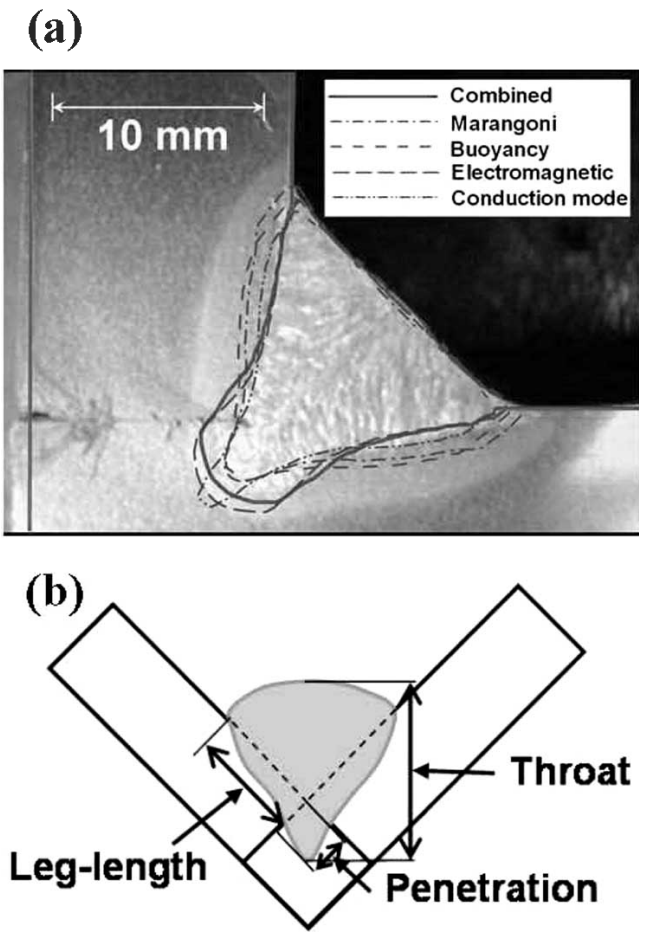

Fig. 2—(*a*) Comparison between the calculated and measured weld-bead profiles. The weld-bead geometry was calculated considering the separate effects of conduction mode of heat transfer, convection due to effect of electromagnetic force, buoyancy, Marangoni force, and the combined convection and conduction mode of heat transfer. The weld-bead profile computed by considering the combined convection and conduction mode of heat transfer matches fairly close to the experimentally measured weld-bead profile. Welding conditions are the same as those in Figure 1(*b*) During the GMA fillet welding process, the weld geometry is commonly specified by three quantities that affect the joint properties: penetration, throat, and leg length.

from the center to the edge of the pool in the region close to the heat source, where the spatial variation of the surface temperature is relatively high. This is due to the negative value of the temperature coefficient of surface tension ($d\gamma/dT$) for the A-36 steel (Table I). In the rear part of the weld pool, where the temperature gradient is relatively low, the effect of Marangoni shear stress is less pronounced than that of electromagnetic force. As a result, the liquid metal flows inward in the rear part of the pool. Due to the difference in flow patterns resulting from Marangoni and electromagnetic forces, the leg length of the weld pool is decreased, while the throat is increased, as shown in Figure 2. The buoyancy force also shows the same trend as Marangoni convection, but its effect is less pronounced due to its small magnitude in comparison with the Marangoni force.[1,2,6] On the other hand, heat transfer in the conduction mode with no fluid-flow calculations provides a hemispherical weld-pool shape at the top with a narrow penetration due to droplets. A comprehensive calculation of heat transfer and fluid flow in the weld pool after considering all the driving

forces provides a fairly good agreement between the computed weld geometry and the experimentally obtained weld geometry (Figure 2(a)). However, some discrepancy between the experimental bead profile and the computed results observed in Figure 2(a) is due to uncertainty in the values of the arc efficiency, effective thermal conductivity, effective viscosity, and the thermal-stress-induced distortion in the welded plates.

B. *Improvement in the Reliability of the Heat-Transfer and Fluid-Flow Calculations*

A reliable forward model provides a useful link between the welding variables and the weld attributes. The heat-transfer and fluid-flow calculations of GMA fillet welding require many input variables, out of which the values of arc efficiency, effective thermal conductivity, and effective viscosity are uncertain. These values are properties of the specific welding system and cannot be easily assigned from fundamental principles. The reliability of the numerical heat-transfer and fluid-flow calculation during GMA fillet welding was enhanced by coupling it with an optimization scheme based on the conjugate-gradient method to estimate the unknown values of arc efficiency (η), effective thermal conductivity (k_e), and effective viscosity (μ_e) using a limited volume of experimental data.[7,18,20] The experimental data used for estimating the values of these unknown parameters are listed in Table II. For simplicity, we assume the following linear relations[18,20] between these unknown variables and the heat input:

$$\eta = g_1 + g_2 \cdot P_e^* \quad [8]$$

$$k_e = g_3 \cdot k_L + g_4 \cdot k_L \cdot P_i^* \quad [9]$$

$$\mu_e = g_5 \cdot \mu_L + g_6 \cdot \mu_L \cdot P_i^* \quad [10]$$

$$P_e^* = \frac{IV/(\pi r_w^2 w_f)}{[\rho c_p (T_L - T_a) + \rho L]} \text{ and}$$

$$P_i^* = \frac{IV/(\pi r_b^2 U_w)}{[\rho c_p (T_L - T_a) + \rho L]} \quad [11]$$

Table II. Welding Conditions Used in the Experiments

Case	Contact Tube to Workpiece Distance (mm)	Wire Feeding Rate (mm/s)	Travel Speed (mm/s)	Voltage (V)	Estimated Current (A)
1	22.2	169.3	4.2	31	312.0
2	22.2	211.7	6.4	31	362.0
3	22.2	169.3	6.4	33	312.0
4	22.2	211.7	4.2	33	362.0
5	28.6	169.3	6.4	31	286.8
6	28.6	169.3	4.2	33	286.8
7	28.6	211.7	4.2	31	331.4
8	28.6	211.7	6.4	33	331.4

Polarity: Direct current, electrode positive.
Joint type: Fillet joint, flat position, 90-deg joint angle, and no root gap.
Electrode type: 1.32-mm- (0.052-in.-) diameter solid wire.
Base metal: ASTM A-36 mild steel.
Shielding gas: Ar-10 pct% CO_2.

where k_L is the conductivity of the liquid material, μ_L is the viscosity of the liquid material, I is the current, V is the voltage, r_w is the wire radius, w_f is the wire feeding rate, ρ is the density, c_p is the specific heat, T_L is the liquidus temperature, T_a is the ambient temperature, L is the latent heat of the alloy, r_b is the arc radius, U_w is the welding speed, and g_1, g_2, g_3, g_4, g_5, and g_6 are constants. In order to calculate the values of the arc efficiency, effective thermal conductivity, and effective viscosity, we require values of the constant terms, *i.e.*, g_1, g_2, g_3, g_4, g_5, and g_6 in Eqs. [8] through [11]. To find the values of these terms, an objective function of the form of a least-squares error is minimized, which depicts the difference between the computed and measured values of the penetration, throat, and leg length defined in Figure 2(b) for various welding conditions.[18] The computed optimal value of these uncertain parameters can be expressed as[18,20]

$$\eta = 0.31 + 4.65 \times 10^{-6} \frac{IV}{w_f} \quad [12]$$

$$k_e = 41.80 + 3.17 \times 10^{-5} \frac{IV}{U_w} \text{ (W/m K)} \quad [13]$$

$$\mu_e = 0.016 + 1.05 \times 10^{-8} \frac{IV}{U_w} \text{ (kg/m s)} \quad [14]$$

where I is the current (in amps), V is voltage (in volts), w_f is the wire feeding speed (in m/s), and U_w is the welding speed (in m/s). The values of η, k_e and μ_e are calculated from Eqs. [12] through [14] for the experimental conditions given in Table II. The optimized values indicate enhancement factors (*i.e.*, $f_k^e = k_e/k_L$) for thermal conductivity and viscosity (*i.e.*, $f_\mu^e = \mu_e/\mu_L$) to be in the range of 5 to 9, as shown in Figure 3. This behavior is consistent with the presence of turbulent flow in the weld pool during GMA welding, as reported in the literature.[5,34–37] Hong *et al.*[35,36] suggested an enhancement factor between 12 and 15 for thermal conductivity and a factor more than 6 for the viscosity for gas

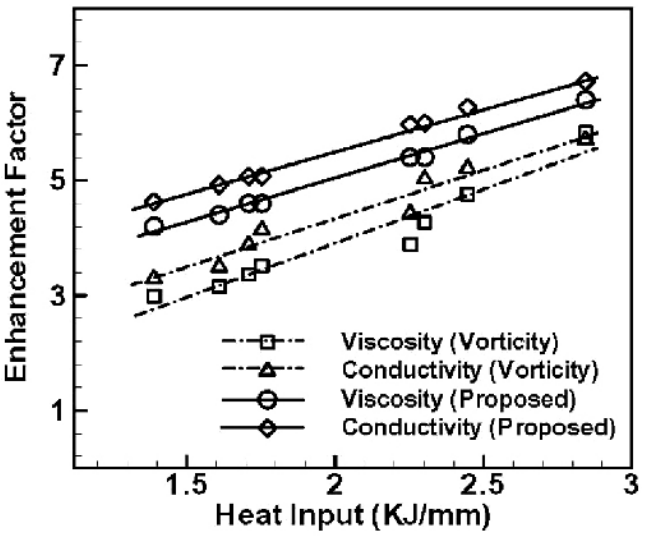

Fig. 3—Computed values of the enhancement factor for thermal conductivity and viscosity using estimated values of unknown parameters by using the proposed phenomenological model and vorticity-based turbulence model for the different welding conditions listed in Table II.

tungsten-arc welding using a 150 A current and 25 V, based on peak-temperature analysis in the weld pool and k-ε turbulence-model calculations. Choo and Szekely[34] suggested an enhancement factor of 8 for the thermal conductivity and a factor of 30 for the viscosity at a current of 100 A by matching the calculated weld-pool geometry with the experimentally determined geometry. They also verified the weld-pool shape and values of enhancement factors using the k-ε turbulence model. The values available in the literature[21,22,34–37] are specific to the welding procedure and the specific welding conditions. Because of the scarcity of data, the available literature cannot be used as a basis for the selection of enhanced transport parameters for any specific welding conditions. The proposed expressions for the calculation of η, k_e, and μ_e given by Eqs. [12] through [14] are valid for the experimental conditions given in Table II for GMA fillet welding in the spray mode.

A vorticity-based mixing-length turbulence model was also used to calculate the values of the effective viscosity and effective thermal conductivity in the weld pool. The mixing length was calculated in the present work using the Van Driest model,[28,29] which can accommodate local variations of the mixing length in a weld pool of an irregular-geometry-containing finger penetration. According to this model, the mixing length at distance of y from the weld-pool boundary is given by

$$l_{\text{mix}} = \kappa y[1 - e^{-y^+/A_o^+}] \qquad [15]$$

The values of the constants κ and A_o^+ used in Eq. [10] are 0.41 and 26.0, respectively,[28,29] whereas the nondimensional distance (y^+) from the weld-pool boundary is calculated as follows:[29]

$$y^+ = y\sqrt{\frac{\rho}{\mu}\left(\frac{\partial u}{\partial y}\right)_w} \qquad [16]$$

The term $(\partial u/\partial y)_w$ in Eq. [16] represents the velocity gradient at the weld-pool boundary. For the three-dimensional flow in the weld pool, the turbulent viscosity is calculated using the Badwin–Lomax model,[28,29] as follows:

$$\mu_T = \rho l_{\text{mix}}^2 |\omega| \qquad [17]$$

where $|\omega|$ is the magnitude of the vorticity vector, given by

$$\omega = \left[\left(\frac{\partial v}{\partial x} - \frac{\partial u}{\partial y}\right)^2 + \left(\frac{\partial w}{\partial y} - \frac{\partial v}{\partial z}\right)^2 + \left(\frac{\partial u}{\partial z} - \frac{\partial w}{\partial x}\right)^2\right]^{1/2} \qquad [18]$$

The turbulent viscosity field is computed using Eq. [17] after every iteration. The corresponding turbulent thermal-conductivity field is updated using a Pr value computed by the model. Figure 3 shows the calculated enhancement factors (*i.e.*, $f_k^e = 1 + k_T/k_L$) for the thermal conductivity and viscosity (*i.e.*, $f_\mu^e = \mu_e/\mu_L$) as a function of heat input by using the vorticity-based turbulence model and the proposed Eqs. [13] and [14]. The calculated enhancement factors for thermal conductivity and viscosity by using vorticity-based turbulence also increase with an increase in the heat input per unit length as obtained by Eqs. [13] and [14]. The reasons for slightly lower values of the average enhancement factors for thermal conductivity and viscosity by the vorticity-based turbulence model compared to Eqs. [13] and [14] are not known. However, the fact that the values of the constants κ and A_o^+ in Eq. [15] were obtained from experiments in parabolic flows may be a contributing factor.

The optimized values of arc efficiency, effective thermal conductivity, and effective viscosity were used in the heat-transfer and fluid-flow model to calculate the weld geometry, *i.e.*, penetration, throat, and leg length for various welding conditions (Figure 4). These results demonstrate two special features. First, a comparison of the computed and the experimental weld dimensions indicates that the forward model provides both the expected trends and the correct values for various combinations of the welding variables *I, V, U*, and w_f. The agreement provides confidence about the adequacy of quantitative representation of the essential physical processes in the phenomenological model and demonstrates its promise to serve as the main computational engine in the overall goal of systematic tailoring of weld attributes. Second, and more interesting, the results show that a given weld dimension can be obtained using various sets of welding-variable values. Since GA can provide a population of solutions, the heat-transfer and fluid-flow model must be combined with an appropriate GA to tailor weld attributes from scientific principles.

C. *Calculation of the Window of Welding Parameters*

Let us consider an example to illustrate how the overall model to tailor weld geometry from scientific principles works. The task involves three steps. First, a target weld geometry is selected by specifying one set of values for the penetration, throat, and leg length. Second, the model is run to obtain multiple combinations of welding-variable sets to achieve this target geometry. Third and finally, the results obtained from the model are adequately verified. Let us now examine these three steps in detail.

The first step, *i.e.*, the specification of the target geometry, in principle, involves stating any plausible combination of the three weld dimensions, *i.e.*, penetration, throat, and leg length. However, it is useful to specify the weld dimensions from an actual welding experiment as a target geometry. Such a choice provides a useful advantage because one of the solutions, *i.e.*, the welding-variable set used to produce this target geometry, is known. If the model works correctly, the solutions must include a set of welding variables that are fairly close to a set used in the experiment. It should be noted that the ability of the model to produce this solution is only a necessary, but not a fully sufficient, component of the model verification. Since the model produces multiple solutions, other solutions obtained from the model also need to be verified.

The second step, *i.e.*, the operation of the model to tailor weld geometry, starts with specifying a population of 150 potential solutions. Each individual in the population represents a set of randomly chosen values of welding variables. For example, Figure 5(a) depicts the initial values of the individuals, *i.e.*, sets of *I, V, U*, and w_f for each individual solution, with *I* and *V* plotted as their product for accommodating the four welding variables in three-dimensional space. Values of the welding variables *I, V, U*, and w_f were chosen randomly, with values between 250.0 and 400.0 A, 25.0 and 40.0 V, 2.25 and 8.0 mm/s, and 100.0 and 250.0 mm/s, respectively, to maintain diversity of the variable values and explore

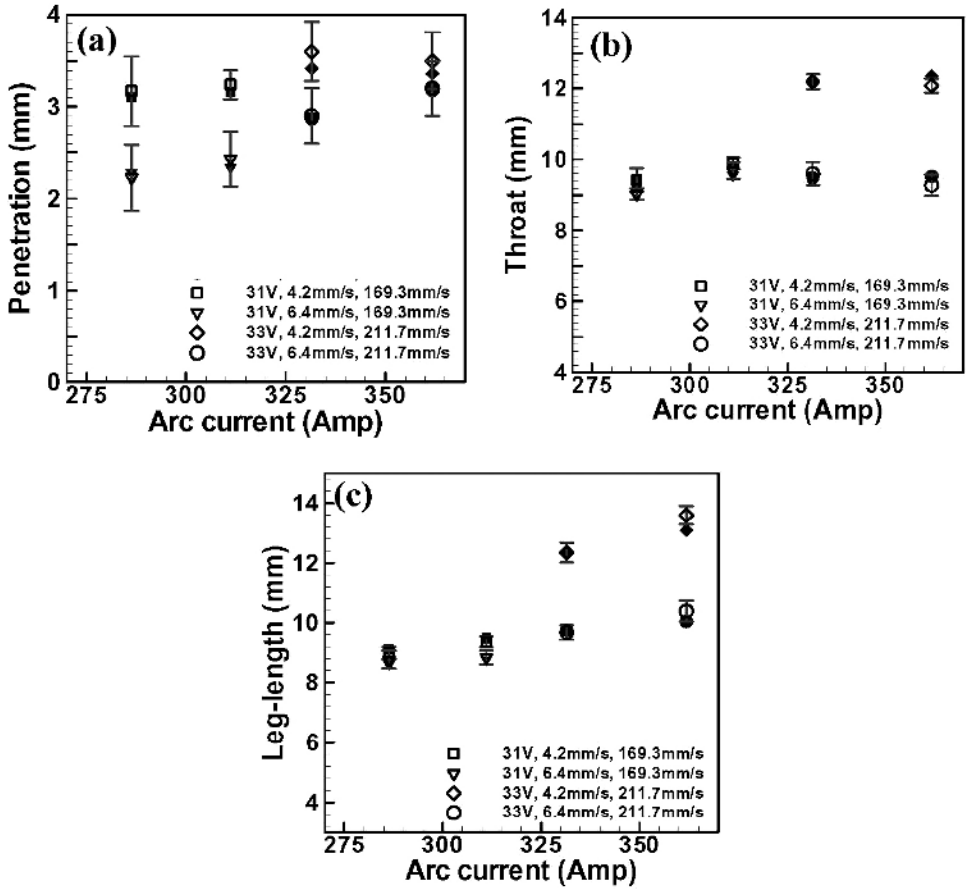

Fig. 4—Weld-bead geometric parameters as a function of welding current: (*a*) penetration, (*b*) throat, and (*c*) leg length. The open symbols represent the experimental results, while the filled symbols indicate the corresponding calculated result. The standard deviations of the experimental data are shown by error bars. The values indicated in the legends represent the arc voltage, welding speed, and wire feed rate, respectively.

a large domain of welding variables to include all possible solutions. These welding-variable sets are then improved iteratively using a combination of the GA and the heat-transfer and fluid-flow model.

The progress of the iterations is monitored by calculating the objective-function values for each set of welding variables (individuals) after each iteration. An individual with a low objective function indicates correct values of the current, voltage, welding speed, and wire feed rate that result in low error between the computed and the target weld geometry. For example, Figure 5(b) shows the computed values of the objective functions for all the individuals depicted in Figure 5(a). The plot shows that for many sets of welding variables, the values of the objective function are fairly low, indicating that each of these welding-variable sets can produce a weld geometry that is close to the target geometry. Figures 6(a) through (c) indicate several clusters of welding-variable combinations that have objective-function values lower than 0.1, 0.008, and 0.004, corresponding to the beginning, fifth generation, and tenth generation of individuals, respectively. What is of special interest in Figure 6 is that sets of welding variables are distributed throughout the welding-variable space, signifying the existence of multiple paths to attain the target geometry. Improved solutions are obtained with iterations (or generations), as observed from the reduction of the values of the objective function of the best individuals. When the values of the objective functions are low and they do not decrease further with iterations, the computed welding-variable sets constitute the final solutions, and these are presented in Table III.

The third and the last step involves verification of the computed solutions. Since the target weld geometry was produced by an experiment, a preliminary test is to check if the population of solutions produced by the model includes an individual set of welding variables that is very close to, if not the same as, that used to produce the weld. These experimental welding variables are presented in Table III together with the computed optimum welding-variable sets. The table shows that the computed values of current, voltage, welding speed, and wire feed rate in the individual "solution (b)" in the table all lie within less than 1 pct of the corresponding experimental welding variables. However, the model also predicted other individual solutions, listed as solutions (a) through (f) in the table. The accuracy of these individual solutions was examined by calculating the weld geometry for each welding-variable set (solutions (a) through (f)) in Table III and comparing the computed weld dimensions with that obtained experimentally. The comparisons, shown in Figures 7(a) through (f), between the computed and the experimental weld dimensions show that the individual welding-variable sets resulted in correct predictions of the weld shape and size as measured by the penetration, throat, and leg length in each

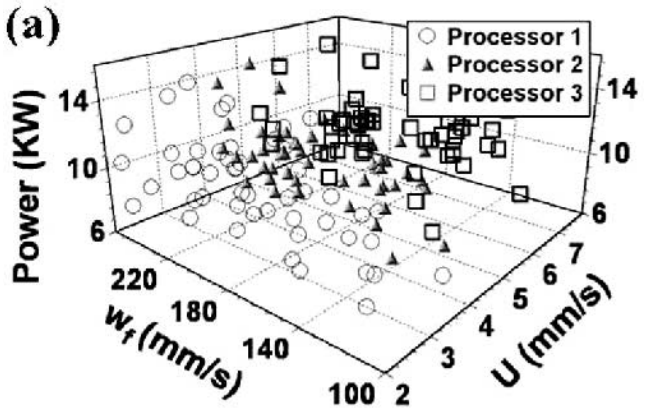

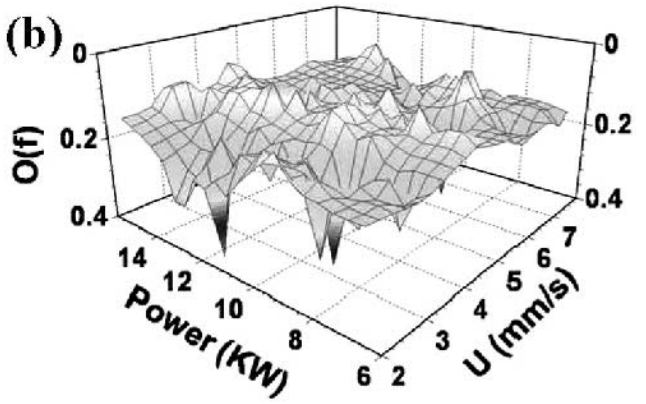

Fig. 5—Initial values of individual welding-variable sets and their objective functions. (*a*) A large space of variables was searched to find optimum solutions, as shown by the 150 randomly selected initial welding-variable sets. (*b*) The low values of the objective functions of several individuals in the initial population indicate the possibility of the existence of multiple optimal solutions. The computational task was divided among three parallel processors to expedite calculations.

case. The values of the four welding variables listed in Table III differ from each other considerably. For example, the voltage, current, welding speed, and wire feed rate values vary between solutions by 38, 12, 47, and 50 pct, respectively. In solutions (a) and (f), the powers required to achieve the target geometry were 9.7 and 14.2 kW, respectively. Furthermore, other welding parameters such as the welding speed and the wire feed rate were also significantly different in the two solutions. All these differences in the important welding variables indicate significant diversity in the paths, all of which lead to the same set of target weld dimensions.

IV. SUMMARY AND CONCLUSIONS

The conventional heat-transfer and fluid-flow models of fusion welding were restructured to enhance the reliability of their predictions and to achieve the bidirectional capability necessary to calculate the welding conditions needed to obtain a target weld geometry. Furthermore, by using a real-number-based GA in the proposed model, multiple sets of welding variables, each of which can lead to a target weld geometry, have been calculated.

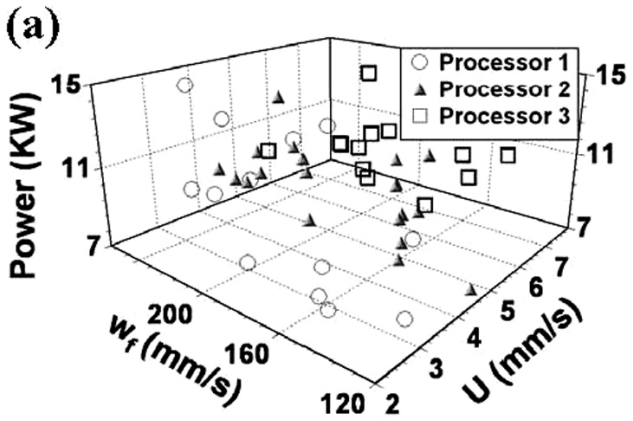

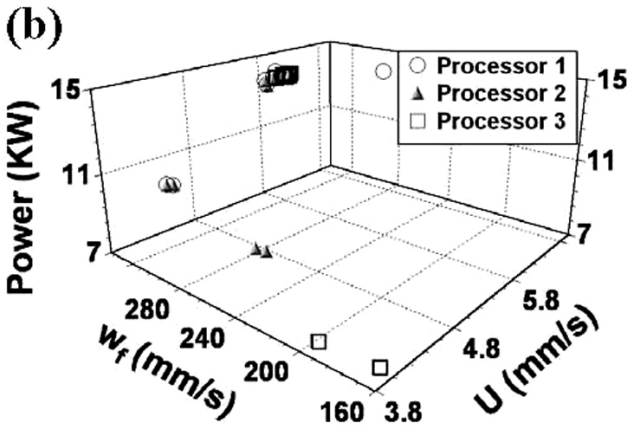

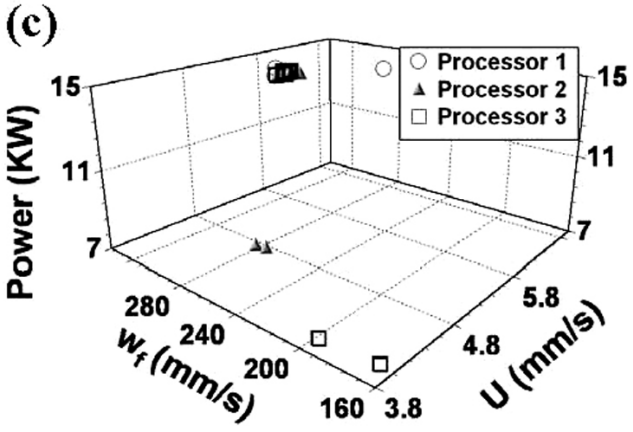

Fig. 6—Several fairly diverse welding-variable sets could produce low values of the objective function, indicating the existence of alternate paths to obtain the target weld geometry. The plots show the welding-variable sets that produced low values of the objective function with iterations. (*a*) initial individuals with $O(f)$ less than 0.1, (*b*) individuals after five iterations with $O(f)$ less than 8.0×10^{-3}, and (*c*) individuals after ten iterations with $O(f)$ less than 4.0×10^{-3}. The computational task was divided among three parallel processors to expedite calculations.

Table III. Optimized Window of Welding Parameters, *i.e.*, Arc Current, Arc Voltage, Welding Speed, and Wire Feed Rate, to Achieve the Following Target Weld Dimensions: Penetration = 3.8 mm, Throat = 11.0 mm, and Leg Length = 12.5 mm; the Target Weld Geometry was Obtained Experimentally Using the Following Welding Variables: I = 331.4 A, V = 31 V, U = 4.2 mm/s, and w_f = 211.7 mm/s

Individual Solutions	I (Amp)	V (Volt)	U (mm/s)	w_f (mm/s)
(a)	315.0	30.7	4.1	239.3
(b)	330.0	31.2	4.2	212.1
(c)	331.5	30.2	4.0	228.4
(d)	321.5	30.7	4.1	239.2
(e)	354.0	31.4	4.1	230.4
(f)	338.0	41.9	5.9	319.2

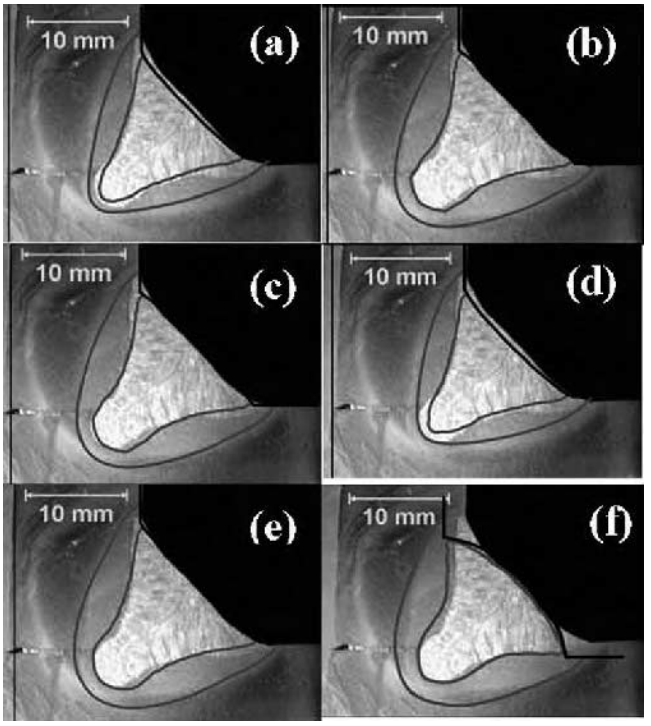

Fig. 7—Comparisons between the calculated and the desired weld-bead geometry for different optimum combinations of welding parameters. The results show that a target geometry can be obtained *via* multiple paths. The inner isotherm (1745 K) represents the calculated weld-pool boundary. The outer isotherm represents 1100 K.

The reliability of the numerical heat-transfer and fluid-flow model was enhanced by coupling it with a conjugate-gradient optimization method for searching and optimizing the values of uncertain welding variables from a limited volume of experimental data. The values of three variables (the arc efficiency, effective thermal conductivity, and effective viscosity) were estimated as a function of welding conditions for GMA welding in the spray mode. The turbulent convection in the weld pool is simulated by a vorticity-based one-equation turbulence model. This turbulence model uses a variable mixing length to adequately consider an irregular and complex weld-pool geometry characterized by finger penetration and severe deformation of the weld pool under the arc. A fair agreement was obtained between predictions of the turbulence model and optimized values of the effective viscosity and effective thermal conductivity. Using the optimized values of unknown parameters, the calculated shape and size of the fusion zone, the finger penetration characteristic of the GMA welds, and the solidified free-surface profile were calculated for several welding conditions. Good agreement between the model predictions and the experimental data of leg length, penetration, and throat for various welding conditions show that this approach is promising.

The bidirectional capability was built into the model by combining the reliable heat-transfer and fluid-flow model with a GA. Unlike conventional heat-transfer and fluid-flow models, which predict weld geometry for a particular set of welding conditions, the proposed model can estimate the welding conditions necessary for obtaining a target weld geometry. Furthermore, the genetic algorithm in the proposed model enables calculation of multiple paths, *i.e.*, several sets of arc currents, arc voltages, welding speeds, and wire feed rates, each of which can lead to a target weld geometry. Although the work reported here focuses on tailoring of weld geometry from scientific principles, these results provide hope that with the development of new methodologies at the crossroads of basic and applied sciences, the promise of science-based tailoring of other features of structure and properties of weldments may also become attainable in the future.

ACKNOWLEDGMENTS

This research was supported by a grant from the United States Department of Energy, Office of Basic Energy Sciences, Division of Materials Sciences, under Grant No. DE-FGO2-01ER45900. Mr. Amit Kumar gratefully acknowledges the award of a fellowship from the American Welding Society. We have received helpful comments from Professors L.Q. Chen, W.M. Small, and R. Roy, Penn State University, and from Dr. S.A. David, Oak Ridge National Laboratory, during preparation of this manuscript.

APPENDIX

PCX-based G3 GA

The GA used in the present study is a PCX operator–based G3 model.[26,27,28] To reduce the computation time, the model is parallelized to run on multiple processors simultaneously. The multiple island (or deme)–based parallelized GA model[24,33] is used to achieve a rapid search for the multiple sets of welding variables by dividing the search space into multiple islands. Rapid convergence is achieved when each island is assigned to a separate processor, because the size of each island is smaller than the total population. After each iteration, a few solutions, selected based on their fitness or objective-function value, are allowed to migrate to other islands.[33] The migration of the best individuals to replace the worst individuals in the neighboring processors (islands) enhances the speed of convergence.[33] The steps involved in the calculations are as follows.

(1) A population is a collection of many individuals, and each individual represents a set of randomly chosen values of the four nondimensionalized welding variables. A parent

refers to an individual in the current population. The best parent is the individual that has the best fitness value, *i.e.*, gives the minimum value of the objective function, defined by Eq. [6], in the entire population. The best parent and two other randomly selected parents are chosen from the population.

(2) From the three chosen parents, two offsprings or new individuals are generated using a recombination scheme. The PCX-based G3 models are known to converge rapidly when three parents and two offsprings are selected.[27] A recombination scheme is a process for creating new individuals from the parents.

(3) In each island, two new parents are randomly chosen from the current population of the island.

(4) A subpopulation of four individuals that includes the two randomly chosen parents in step 3 and the two new offsprings generated in step 2 is formed.

(5) The two best solutions, *i.e.*, the solutions having the least values of the objective function, are chosen from the subpopulation of the four members created in step 4. These two individuals replace the two parents randomly chosen in step 3.

(6) If the sum total of the objective functions of all individuals in all islands does not significantly change with iterations, each island exports five best individuals to the two other processors and simultaneously receives ten individuals from other islands. Each island then discards the ten individuals with the highest values of objective functions. This procedure conserves the same number of individuals in each generation. The calculations are repeated from step 1 again, until convergence is achieved.

The aforementioned steps, as applied to the present problem, are shown in Figure 8. Figure 9 illustrates the working of the model to find the window of welding parameters to achieve a target weld geometry. The recombination scheme (step 2) used in the present model is based on a PCX operator.[26,27,28] A brief description of the PCX operator,[26,27,28] as applied to the present problem, is presented as follows.

First three parents, *i.e.*, $\left(f_1^0, f_2^0, f_3^0, f_4^0\right)$, $\left(f_1^1, f_2^1, f_3^1, f_4^1\right)$, and $\left(f_1^2, f_2^2, f_3^2, f_4^2\right)$, are randomly selected from the current population. Here, the subscripts represent the four variables or the welding parameters, while the superscripts denote the parent identification number. The mean vector or centroid, $\mathbf{g} = \left(\frac{f_1^0 + f_1^1 + f_1^2}{3}, \frac{f_2^0 + f_2^1 + f_2^2}{3}, \frac{f_3^0 + f_3^1 + f_3^2}{3}, \frac{f_4^0 + f_4^1 + f_4^2}{3}\right)$, of the three chosen parents is computed. To create an offspring, one of the parents, for example, $\mathbf{x}^{(p)} = (f_1^0, f_2^0, f_3^0, f_4^0)$, is chosen randomly. The direction vector, $\mathbf{d}^{(p)} = \mathbf{x}^{(p)} - \mathbf{g}$, is next calculated from the selected parents to the mean vector or centroid. Thereafter, from each of the other two parents, *i.e.*, $(f_1^1, f_2^1, f_3^1, f_4^1)$ and $(f_1^2, f_2^2, f_3^2, f_4^2)$, perpendicular distances (D_i) to the direction vector ($\mathbf{d}^{(p)}$) are computed and their average ($\bar{D}$) is found. Finally, the offspring, *i.e.*, $\mathbf{y} = (f_1', f_2', f_3', f_4')$, is created as follows:

$$\mathbf{y} = \mathbf{x}^{(p)} + w_\zeta \left|\mathbf{d}^{(p)}\right| + \sum_{i=1, i\neq p}^{4} w_\eta \bar{D}\, \mathbf{h}^{(i)} \qquad [A1]$$

where $\mathbf{h}^{(i)}$ represents the orthonormal bases that span the subspace perpendicular to $\mathbf{d}^{(p)}$, and w_ζ and w_η are randomly calculated zero-mean normally distributed variables. The

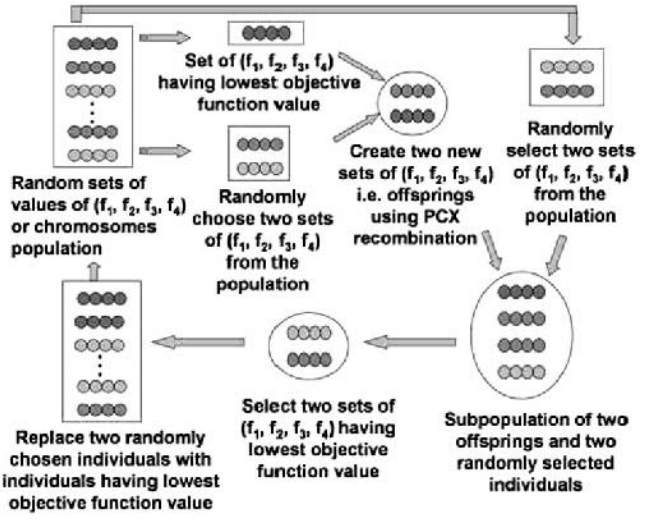

Fig. 8—The G3 model using the PCX operator.

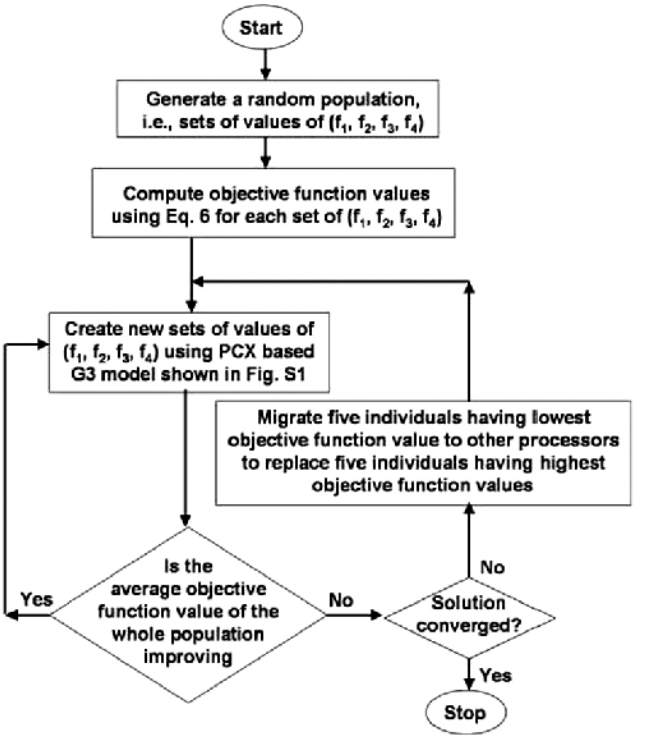

Fig. 9—Flow chart showing the calculation procedure in the parallelized G3 model.

values of the variables that characterize the offspring ($\mathbf{y} = \left(f_1', f_2', f_3', f_4'\right)$) are calculated as follows:

$$f_1' = f_1^0 + f_{11} + f_{12} \qquad [A2a]$$

$$f_2' = f_2^0 + f_{21} + f_{22} \qquad [A2b]$$

$$f_3' = f_3^0 + f_{31} + f_{32} \qquad [A2c]$$

$$f_4' = f_4^0 + f_{41} + f_{42} \qquad [A2d]$$

where

$$f_{11} = w_\zeta \left(\frac{2f_1^0 - f_1^1 - f_1^2}{3}\right) \qquad [A3a]$$

$$f_{21} = w_\zeta\left(\frac{2f_2^0 - f_2^1 - f_2^2}{3}\right) \quad [A3b]$$

$$f_{31} = w_\zeta\left(\frac{2f_3^0 - f_3^1 - f_3^2}{3}\right) \quad [A3c]$$

$$f_{41} = w_\zeta\left(\frac{2f_4^0 - f_4^1 - f_4^2}{3}\right) \quad [A3d]$$

$$f_{12} = w_\eta\left(\frac{a_2 + b_2}{2}\right)\left[1 - \left(\frac{2f_1^0 - f_1^1 - f_1^2}{3d}\right)^2\right] \quad [A3e]$$

$$f_{22} = w_\eta\left(\frac{a_2 + b_2}{2}\right)\left[1 - \left(\frac{2f_2^0 - f_2^1 - f_2^2}{3d}\right)^2\right] \quad [A3f]$$

$$f_{32} = w_\eta\left(\frac{a_2 + b_2}{2}\right)\left[1 - \left(\frac{2f_3^0 - f_3^1 - f_3^2}{3d}\right)^2\right] \quad [A3g]$$

$$f_{42} = w_\eta\left(\frac{a_2 + b_2}{2}\right)\left[1 - \left(\frac{2f_4^0 - f_4^1 - f_4^2}{3d}\right)^2\right] \quad [A3h]$$

The various unknown variables used in Eqs. [A3a] through [A3h] can be represented in simplified form as follows:

$$d = \sqrt{\begin{array}{l}\left(\frac{2f_1^0 - f_1^1 - f_1^2}{3}\right)^2 + \left(\frac{2f_2^0 - f_2^1 - f_2^2}{3}\right)^2 \\ + \left(\frac{2f_3^0 - f_3^1 - f_3^2}{3}\right)^2 + \left(\frac{2f_4^0 - f_4^1 - f_4^2}{3}\right)^2\end{array}} \quad [A4a]$$

$$a_2 = e_1 \times \sqrt{1 - (a_1)^2} \quad [A4b]$$

$$b_2 = e_2 \times \sqrt{1 - (b_1)^2} \quad [A4c]$$

$$a_1 = \sum_{i=1}^{i=4} \frac{\left(f_i^1 - f_i^0\right)\left(\frac{2f_i^0 - f_i^1 - f_i^2}{3}\right)}{d \times e_1} \quad [A4d]$$

$$e_1 = \sqrt{\left(f_1^1 - f_1^0\right)^2 + \left(f_2^1 - f_2^0\right)^2 + \left(f_3^1 - f_3^0\right)^2 + \left(f_4^1 - f_4^0\right)^2} \quad [A4e]$$

$$b_1 = \sum_{i=1}^{4} \frac{\left(f_i^2 - f_i^0\right)\left(\frac{2f_i^0 - f_i^1 - f_i^2}{3}\right)}{d \times e_2} \quad [A4f]$$

$$e_2 = \sqrt{\left(f_1^2 - f_1^0\right)^2 + \left(f_2^2 - f_2^0\right)^2 + \left(f_3^2 - f_3^0\right)^2 + \left(f_4^2 - f_4^0\right)^2} \quad [A4g]$$

REFERENCES

1. S.A. David and T. DebRoy: *Science*, 1992, vol. 257, pp. 497-502.
2. T. DebRoy and S.A. David: *Rev. Mod. Phys.*, 1995, vol. 67, pp. 85-112.
3. A. Kumar and T. DebRoy: *J. Appl. Phys.*, 2003, vol. 94, pp. 1267-77.
4. C.H. Kim, W. Zhang, and T. DebRoy: *J. Appl. Phys.*, 2004, vol. 94, pp. 2667-79.
5. W. Zhang, C.H. Kim, and T. DebRoy: *J. Appl. Phys.*, 2004, vol. 95, pp. 5210-19.
6. W. Zhang, C.H. Kim, and T. DebRoy: *J. Appl. Phys.*, 2004, vol. 95, pp. 5220-29.
7. A. Kumar and T. DebRoy: *Int. J. Heat Mass Transfer*, 2004, vol. 47, pp. 5793-806.
8. X. He, P. Fuerschbach, and T. DebRoy: *J. Appl. Phys.*, 2004, vol. 96, pp. 4547-55.
9. X. He, P.W. Fuerschbach, and T. DebRoy: *J. Phys. D: Appl. Phys.*, 2003, vol. 36, pp. 1388-98.
10. H. Zhao and T. DebRoy: *J. Appl. Phys.*, 2003, vol. 93, pp. 10089-96.
11. J.W. Elmer, T.A. Palmer, W. Zhang, B. Wood, and T. DebRoy: *Acta Mater.*, 2003, vol. 51, pp. 3333-49.
12. W. Zhang, J.W. Elmer, and T. DebRoy: *Scripta Mater.*, 2002, vol. 46, pp. 753-57.
13. S. Mishra and T. DebRoy: *J. Phys. D: Appl. Phys.*, 2004, vol. 37, pp. 2191-96.
14. S. Mishra and T. DebRoy: *Acta Mater.*, 2004, vol. 52, pp. 1183-92.
15. T. Hong and T. DebRoy: *Metall. Mater. Trans. B*, 2003, vol. 34B, pp. 267-69.
16. S. Kou: *Welding Metallurgy*, 2nd ed., John Wiley & Sons, New York, NY, 2002, pp. 97-121.
17. W. Zhang, G.G. Roy, J.W. Elmer, and T. DebRoy: *J. Appl. Phys.*, 2003, vol. 93, pp. 3022-33.
18. A. Kumar and T. DebRoy: *J. Phys. D: Appl. Phys.*, 2005, vol. 38, pp. 127-34.
19. H.B. Smartt and C.J. Einerson: *Welding J.*, 1993, vol. 72, pp. 217-29.
20. A. Kumar, W. Zhang, and T. DebRoy: *J. Phys. D: Appl. Phys.*, 2005, vol. 38, pp. 119-26.
21. A. De and T. DebRoy: *J. Appl. Phys.*, 2004, vol. 95, pp. 5230-40.
22. A. De and T. DebRoy: *J. Phys. D: Appl. Phys.*, 2004, vol. 37, pp. 140-50.
23. D.E. Goldberg: *Genetic Algorithm in Search, Optimization and Machine Learning*, Addison-Wesley, Boston, MA, 1989, pp. 25-74.
24. *Handbook of Evolutionary Computations*, T. Back, D.B. Fogel, and Z. Michalewicz, eds., IOP Publishing Ltd., Oxford University Press, Oxford, United Kingdom, 2000, pp. C.1-C6.4.
25. A. Kumar, S. Mishra, J.W. Elmer, and T. DebRoy: *Metall. Mater. Trans. A*, 2005, vol. 36A, pp. 15-22.
26. K. Deb, A. Anand, and D. Joshi: *Evolutionary Computation*, 2002, vol. 10, pp. 371-95.
27. K. Deb: *Multi-Objective Optimization Using Evolutionary Algorithms*, 1st ed., John Wiley & Sons, New York, NY, 2001, pp. 45-80.
28. D.C. Wilcox: *Turbulence Modeling for CFD*, DCW Industries, CA, 1993, pp. 38-52.
29. B.E. Launder and D.B. Spalding: *Lectures in Mathematical Models of Turbulence*, Academic Press, London, 1972, pp. 23-45.
30. S. Kumar and S.C. Bhaduri: *Metall. Trans. B*, 1994, vol. 25B, pp. 435-41.
31. V.R. Voller and C. Prakash: *Int. J. Heat Mass Transfer*, 1987, vol. 30, pp. 1709-19.
32. S.V. Patankar: *Numerical Heat Transfer and Fluid Flow*, Hemisphere, New York, NY, 1980, pp. 41-71.
33. E. Cantú-Paz: *Efficient and Parallel Genetic Algorithms*, Kluwer Academic Publishers, Boston, MA, 2000, pp. 36-72.
34. R.T.C. Choo and J. Szekely: *Welding J.*, 1994, vol. 73, pp. 25-31.
35. K. Hong, D.C. Weckmann, A.B. Strong, and W. Zheng: *Sci. Technol. Welding Joining*, 2002, vol. 7, pp. 125-36.
36. K. Hong, D.C. Weckmann, A.B. Strong, and E. Pardo: *Proc. 1st Int. Conf. on Transport Phenomena in Processing*, S.I. Guceri, ed., Technomic Pub., Lancaster, PA, 1992, pp. 626-35.
37. K. Hong, D.C. Weckmann, A.B. Strong, and W. Zheng: *Sci. Technol. Welding Joining*, 2003, vol. 8, pp. 313-24.